



Article

Complete Desensitization of Aluminum–Magnesium Alloys via Boron Addition

Ramasis Goswami ^{*}, Alex Moser, Ronald L. Holtz [†], Syed B. Qadri [‡] and Andrew Geltmacher

Materials Science and Technology Division, Naval Research Laboratory (NRL), Washington, DC 20375, USA

^{*} Correspondence: ramasis.goswami@nrl.navy.mil

[†] Retired from NRL, Washington, DC 20375, USA.

[‡] Retired Emeritus, NRL, Washington, DC 20375, USA.

Abstract: We address here an important issue related to sensitization effects in Al5083 by mitigating the grain boundary precipitation of the beta phase and demonstrate that the addition of a small amount of boron to Al5083 impedes the precipitation of the beta phase, Al₃Mg₂, also known as the Samson phase. In Al–Mg alloys, the precipitation of Al₃Mg₂ usually occurs at grain boundaries in the temperature range of 50 to 200 °C from a supersaturated solid solution of Al–Mg and makes these alloys susceptible to intergranular corrosion and stress corrosion cracking. Upon boron addition, we show, using transmission electron microscopy, that a diboride phase, AlMgB₂, forms at grain boundaries instead of the beta phase upon extended annealing at 150 °C. This diboride phase does not dissolve in saltwater, suggesting it is less anodic relative to the matrix. To quantify and compare the dissolution characteristics, we carried out nitric acid mass loss test for Al5083 samples containing 3 wt.% boron treated at 190 h at 150 °C, and fully sensitized Al5083 samples containing 0.0 wt.% boron. We estimate the mass loss to be 4 mg/cm² for boron containing samples as compared to the mass loss of 45 mg/cm² for samples without boron, indicating that the addition of boron is highly effective in suppressing the susceptibility to intergranular corrosion in Al5000 series alloys. This provides a potential route to minimize the longstanding problem of ship structure sensitization.

Keywords: Al–Mg alloys; Al5083; Al5456; sensitization; precipitation; microstructure; intergranular corrosion; stress corrosion cracking



Citation: Goswami, R.; Moser, A.; Holtz, R.L.; Qadri, S.B.; Geltmacher, A. Complete Desensitization of Aluminum–Magnesium Alloys via Boron Addition. *Corros. Mater. Degrad.* **2023**, *4*, 317–330. <https://doi.org/10.3390/cmd4020016>

Academic Editor: Angeliki G. Lekatou

Received: 10 April 2023

Revised: 1 June 2023

Accepted: 2 June 2023

Published: 6 June 2023



Copyright: © 2023 by the authors. Licensee MDPI, Basel, Switzerland. This article is an open access article distributed under the terms and conditions of the Creative Commons Attribution (CC BY) license (<https://creativecommons.org/licenses/by/4.0/>).

1. Introduction

Future faster and lighter naval vessels are increasingly relying upon lightweight aluminum alloys as ship structural materials. Aluminum alloys, particularly Al5000 series alloys, are widely used for boat and ship structural applications because they exhibit good weldability, formability, and a high strength to weight ratio. In addition, in their as-received conditions, these alloys exhibit good intergranular corrosion resistance. The as-received condition refers to the samples with H-131 tempered condition. However, these alloys become susceptible to intergranular corrosion (IGC) and stress corrosion cracking (SCC), as a result of thermal exposure in the range of 50–200 °C, which is known as sensitization. The thermal exposure results in the precipitation of the grain boundary beta phase, Al₃Mg₂ from the supersaturated Al–Mg solid solution. The formation of beta phase from the supersaturated Al–Mg solid solution is in general well known and has been reported by several authors [1–7]. It is shown the beta phase is highly anodic relative to the Al matrix, and upon exposure to seawater, the anodic dissolution of the grain boundary beta phase occurs, leading to a structural failure via IGC or SCC.

Al5000 series alloys, such as Al5083 and Al5456, are being used extensively in a number of ships in deck and superstructure plating, including the DDG 963, CG-47, and I-5000 FFG classes, as well as the Littoral Combat Ship (LCS), Joint High-Speed Vessel (JHSV), and Joint Maritime Assault Connector (JMAC) [8]. The sensitization of Al–Mg alloys affects a number

of ships and naval vessels as they experience severe degradation, which is mostly due to an increase in temperature of the deck plate or regions in the vicinity of the engine room. In addition, the operational environments on ships change upon navigation through different regions. It is known the ambient temperature in equatorial regions and in the Persian Gulf can reach 60–80 °C. Under such conditions, sensitization in ship structure is thought to develop slowly, and the materials are only partially or discontinuously sensitized through most of their lifecycle. The degree of sensitization (DOS) can be detected and quantified using the nitric acid mass loss testing (NAMLT) [9].

To achieve a ship structure platform life of 20 to 30 years or more, critical corrosion mitigation strategies are needed for lightweight Al–Mg alloys in the naval environment, which demonstrate significant desensitization against corrosion, SCC, and IGC. Advances in lightweight ship structures may be applied to civilian sea transport as well. Improved lightweight structural materials will allow for faster and more fuel-efficient shipping, increased safety, and lower lifecycle cost due to increased reliability.

These Al–Mg alloys are also used in automotive parts and engines and as heat exchangers in the petroleum industry [10] due to their excellent weldability, high strength-to-weight ratio, and formability. However, welding can cause sensitization in the heat affected zone, which results in IGC in the heat exchangers used even at low temperatures.

Local reversion thermal treatment [11] has been applied to tackle reverse sensitization in sensitized Al–Mg samples. This treatment is equivalent to homogenizing Al–Mg alloys with Mg between 4 to 5 wt.% in the temperature range of 300 to 500 °C for certain durations. Such treatment will dissolve the beta phase and form a fcc solid solution of Al–Mg, which is not a novel process, as it is depicted in the Al–Mg phase diagram. The major limitation of the local reversion treatment, however, is the fact that the samples will become sensitized when they are exposed again to 50–200 °C for some length of time. Based on this type of annealing treatment, two patents have been issued recently. The first one uses pulsed electron beams as a heat source and heats the surface of the sample [8]. This treatment might reduce the amount of beta phase by dissolving the beta phase, although the evidence of the dissolution of beta phase has not been shown in the patent [8]. In addition, the pulsed electron beam might locally melt the sample surface and can generate a heat-affected zone and cause sensitization. Another process involves an annealing and cooling treatment to dissolve the sensitized sample's beta phase in the temperature range of 300 to 340 °C and cooling it slowly (0.5 deg/min) to room temperature [12]. However, these processes do not adequately address the desensitization process of the Al–Mg plates, as the beta phase will regrow at grain boundaries when exposed to temperature of 50 to 200 °C for certain durations.

Accumulative roll-bonding (ARB), which is a deformation process, has been applied to investigate whether it affects the intergranular corrosion (IGC) susceptibility of Al 5083 [13]. This process introduces a high degree of deformation, and as a result, a large amount of β -phase can form. It has been reported that it did not cause an increase in IGC susceptibility due to favorable morphology and a distribution of β -phase in the structure [13]. Although it does not increase the susceptibility of IGC, the samples are still susceptible to IGC and will be in a highly sensitized state. In Al 5083, higher corrosion resistance has been reported with microstructure-containing ultrafine grains (UFG) obtained using a friction stir weld (FSW) process [14,15] and has been linked with the faster passivation/re-passivation kinetics. However, it has been shown that such deformation induced grain size reduction does not suppress the beta phase formation and decrease the IGC susceptibility [5,16].

Several alloy additions, such as Ag, Ce, Cu, Li, Nd, Ni, Sc, Si, Sr, Y, and Zr [17,18] have also been applied to desensitize Al–Mg alloys. In some cases, particularly for Sr and Cu, they resulted in a significant decrease in beta phase fraction. The experimental estimation of the beta phase fraction is usually difficult and could be erroneous based on the contrast and composition information from the beta phase using scanning electron microscopy. For the Sr case, no diffraction evidence was given involving the Al–Mg–Sr phase formation [17]. An Al_2MgCu type of anodic phase [17] can form with Cu addition, which will reduce the

fraction of beta phase. However, most of those alloy additions were not effective as they do not suppress the beta phase formation. The addition of Zn [19] could affect the beta phase formation as it might change the Al 5000 series to Al 7000 series, depending on the amount of added Zn. The addition of Li to Al–Mg results in the Al_2MgLi compound [17], which is a highly anodic phase. Recently, a protective coating based on Zn-based primers has been applied to Al–Mg plates [20] to suppress the IGC and SCC. However, it does not actually address the desensitization of Al–Mg alloys. However, the primer topcoat can fail during service, exposing the sensitized Al–Mg plates for severe IGC.

The present approach focuses on preventing the nucleation of the beta phase at grain boundaries by alloying with a small amount of boron. The alloy addition would modify the grain boundary characteristics by segregating on grain boundaries to form di-boride with Al and Mg. Our initial studies [21–23] show that a small addition of boron to Al–Mg alloy results in the formation of AlMgB_2 . The AlMgB_2 phase formation decreases the nucleation rate of the beta phase as well as the supersaturation level of Mg in an Al matrix, which is a driving force for the formation of beta phase in Al–Mg alloys. The objective of this work is to mitigate the degradation in Al5083 by modifying the existing Al 5083 with the addition of boron, which suppresses the beta phase at the grain boundaries. In our case, the beta phase will never form during service or with repeated thermal exposure between 50 to 200 °C.

2. Experimental Methods

Arc melting was used to produce ingots of Al 5083-boron (each ingot weight: ~10 gm) in an inert atmosphere. To ensure homogeneity, such ingots were arc-melted several times and cooled in the furnace. For Al 5083-boron, four different alloys with 0.5, 1, 2, and 3 wt.% boron were prepared. The as-received commercial Al5083 contains mostly 4.00 to 4.9 wt.% Mg, 0.4 to 1.0 wt.% Mn, 0.4 wt.% Fe, 0.1 wt.% Cu, 0.4 wt.% Si, 0.25 wt.% Zn, 0.15 wt.% Ti, and 0.05–0.25 wt.% Cr, and the balance is Al. Commercial Al5083 alloys were fully sensitized at 100 and 175 °C. The alloys containing boron were then homogenized at 500 °C for an hour and annealed at 150 °C for 190 h. A Rigaku X-ray diffraction (XRD) unit with $\text{Cu-K}\alpha$ radiation was employed to identify different phases in the composites. For transmission electron microscopic (TEM) observations, samples were prepared using a precision Gatan ion mill with a gun voltage of 4 kV and a sputtering angle of 10°. A JEOL-2200FX analytical transmission electron microscope was then used to investigate the microstructure and composition of samples. Fine probe energy dispersive X-ray spectroscopy (EDS) was used to study the distribution of boron, magnesium, and aluminum. In addition, high angle annular dark field (HAADF) imaging was used to investigate the microstructure. Vickers hardness testing was performed with a 200 gm load and a dwelling time of 15 s. Stress corrosion cracking (SCC) studies were carried out with a constant crack opening displacement in the S–L orientation on pre-cracked double cantilever beam (DCB) specimens, and saltwater (3 wt.%) was added drop wise throughout the SCC experiment. The degree of sensitization (DOS) was measured with the ASTM G67 Nitric Acid Mass Loss Test. For this test, samples with 3 wt.% boron and samples containing no boron were immersed at room temperature in concentrated nitric acid for 24 h. The sample weight per unit area was measured after the test and compared with the weight per unit area before the test. In addition, the dissolution studies were carried out for almost a week in 3 wt.% saltwater at room temperature for a week for samples containing boron and samples without boron. These samples were then observed using optical and scanning electron microscopy (SEM). In addition, to observe the dissolution of the beta phase at grain boundaries, thin TEM foils were immersed in 3 wt.% saltwater for two minutes at room temperature. In this case, TEM samples were not mounted on a Cu grid.

3. Results and Discussion

Here, we initially present results on as-received Al5083 (H-131) and sensitized Al5083 samples, which were fully sensitized at 100 and 175 °C. A TEM image of the as-received sample, showing a grain boundary with no beta phase, is given in Figure 1a. It contains Al–Mn–Fe–Cr type dispersoids mostly within the matrix (see Figure 1b). In some cases, these dispersoids have also been observed at grain boundaries [2]. In Figure 1c–e, we show the distribution of Mg, Al, and Mn, respectively, from these dispersoids within a grain. Most commercial Al–Mg alloys (Al 5053 and Al 5456) contain 4 to 6 wt.% Mg. During the casting of Al–Mg alloys, the liquid Al (Mg) with 4 to 6 wt.% Mg transforms into a supersaturated solid solution during cooling to room temperature. The Al (Mg) supersaturated solid solution then decomposes to an Al (Mg) + beta phase with continued exposure between 50 to 200 °C.

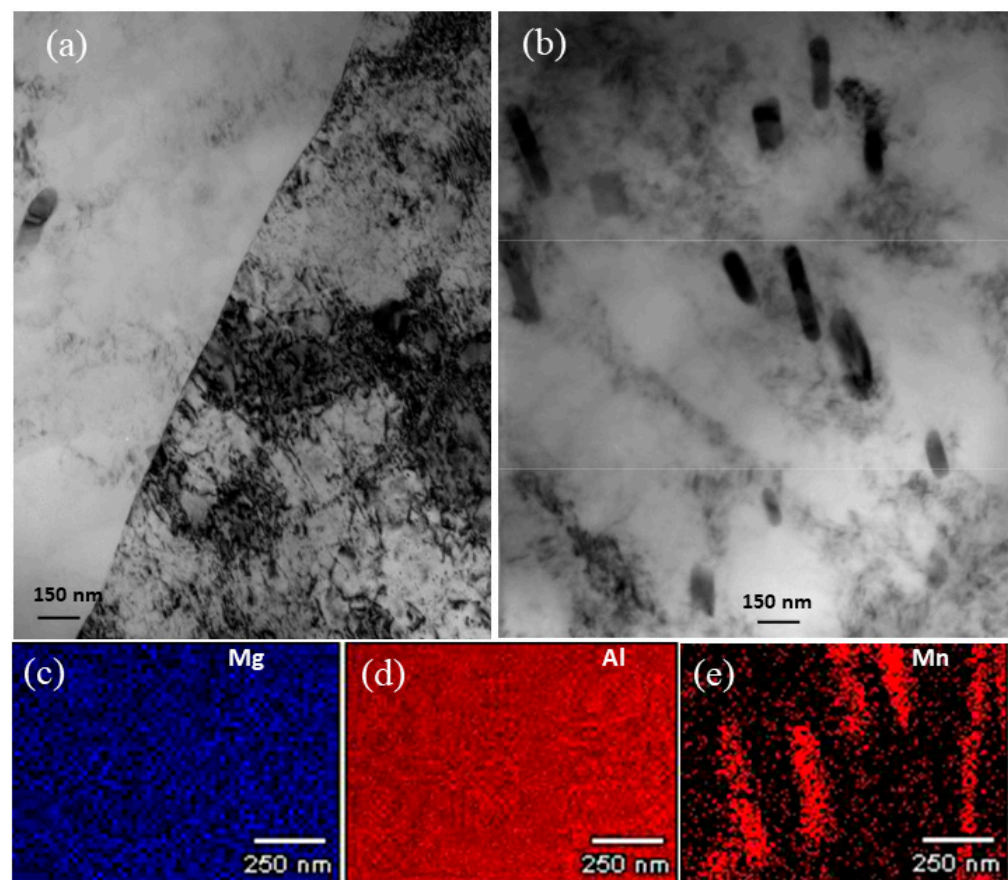


Figure 1. (a) TEM image showing a grain boundary of Al 5083 in the as-received condition with no beta phase. (b) TEM image showing Al–Mn–Fe–Cr-based dispersoid particles with an Al 5083 grain. (c–e) The fine probe EDS maps showing the distribution of Mg, Al, and Mn of the dispersoid particles, respectively.

For the samples fully sensitized at 175 °C for ~150 h, the TEM image shows the formation of the beta phase at a grain boundary (see Figure 2a). A thin denuded zone (bright contrast) close to the grain boundary beta phase can be observed. Fine probe EDS maps (Figure 2b–d) were obtained from this region, showing the distribution of Mg, Al, Mn, and Cr, respectively. It clearly shows that the beta phase formed at the grain boundary contains mostly Al and Mg, as the count of Mn and Cr in the EDS maps at the grain boundary phase is almost zero.

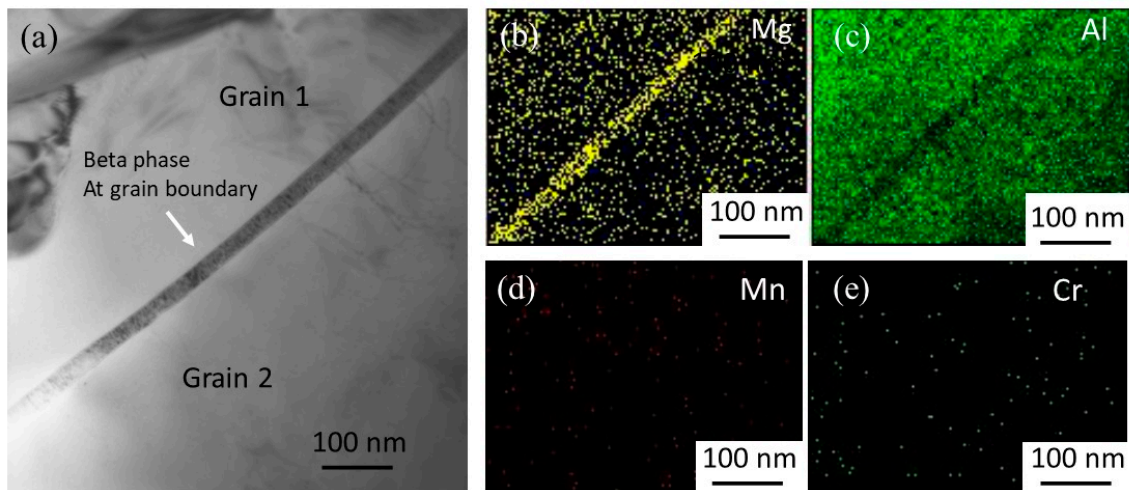


Figure 2. (a) TEM image showing the grain boundary beta phase in sensitized Al 5083. (b–e) The corresponding fine probe EDS maps showing the distribution of Mg, Al, Mn, and Cr, respectively.

To investigate the dissolution behavior of the beta phase, we conducted the SEM imaging of the fully sensitized sample at 175 °C before and after immersing the sample in saltwater. Figure 3a is a SEM image phase showing the beta phase at a grain boundary and within the grains as well as before immersion. Note here the beta phase within a grain forms on top of the Al–Mn–Fe–Cr type intermetallic. This sample was immersed in saltwater for a week, and one could observe the dissolution of the beta phase at the grain boundary (see Figure 3b). In addition to grain boundary dissolution, the dissolution can be observed with grains, as well as forming a large number of fine pits. We also immersed TEM samples in a fully sensitized state with continuous beta phase at grain boundaries to saltwater for 2 min and observed that the beta phase was completely removed and assumed to be dissolved in saltwater (see Figure 3c). One could see an Al–Mn–Fe–Cr type dispersoid particle at the boundary, which was not dissolved. We carried out the SCC characterization of both the as-received Al-5083 (H-131) and the sensitized samples. The threshold stress intensity factor (K_{ISCC}) for the as-received sample is 18.7 MPa \sqrt{m} [2]. The stress intensity factor was observed to decrease considerably to 2.2 MPa \sqrt{m} in the sensitized condition [2]. The fracture surface of stress corrosion cracked sample in fully sensitized condition is intergranular (Figure 3d) as a result of the dissolution of the anodic beta phase at the grain boundaries. Note one could observe the elongated granular morphology in the fracture surface in the S–L orientation.

The crystal structure of the beta phase (space group: Fd-3m, no. 227) is complex and has an fcc crystal structure with 1168 atoms per unit cell. The lattice parameter, $a = 28.44 \text{ \AA}$, is ~ 7 times greater than the lattice parameter of Al [24,25]. The structure containing such a huge number of atoms was identified by Samson using X-ray diffraction. Later, this phase was named after Samson and termed the Samson phase. In Figure 4a, we present a HRTEM image of the Samson phase of as-cast Al-30 wt.% Mg close to the (110) zone showing the (111) lattice planes and faults. The fast Fourier transform (FFT), Figure 4b, was generated from the HRTEM image, showing the series of 111 reflections along with (777) as shown by arrows. The (088) spot, similar to the (022) series spots, is also indicated by an arrow. The d-spacing of the (111) beta phase is 16.3 \AA , suggesting that the d-spacing of the (777) reflection of the beta phase, 2.345 \AA , is close to the d-spacing of (111) Al. We have not observed any unique orientation relationship between the Al matrix and the beta phase. In some cases, the (088) reflection was observed as being nearly parallel to 111 of Al. Figure 5a is a HRTEM image in the (110) zone of both the beta phase and Al, showing that the (088) plane of the beta phase and (111) Al plane is nearly parallel. The FFT from both phases is shown in Figure 5b.

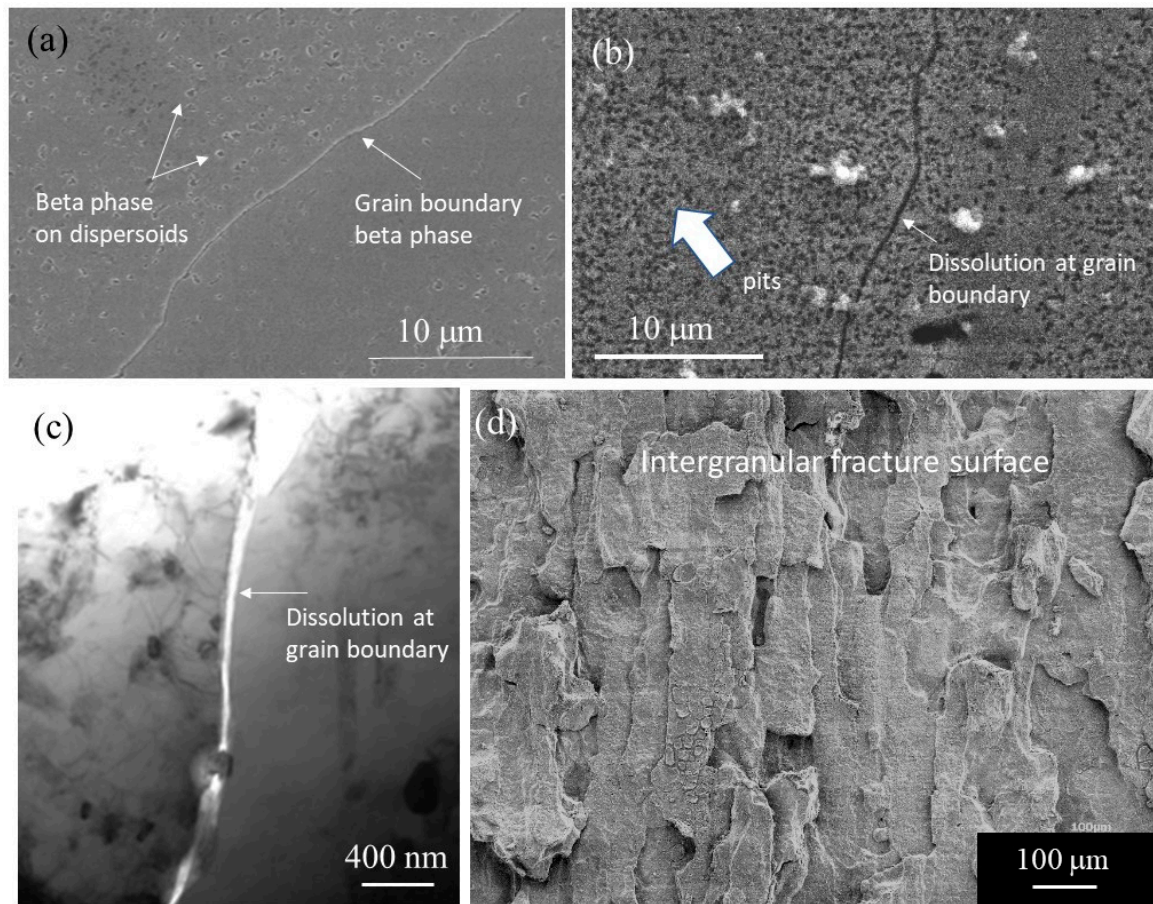


Figure 3. (a) SEM image of the sensitized Al 5083 showing beta phase at grain boundary and within grains. (b) SEM image showing the grain boundary dissolution and high density of pits within grains. (c) TEM image showing the dissolution of grain boundary beta phase. (d) SEM image showing intergranular fracture surface.

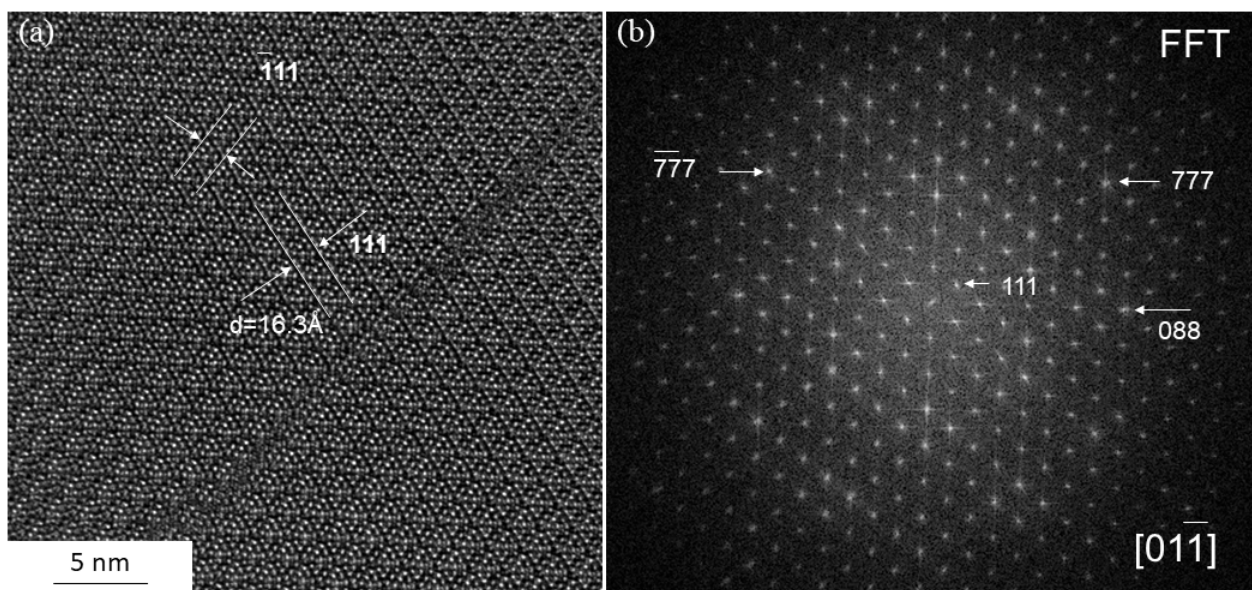


Figure 4. (a) HRTEM image of the beta phase in the (01-1) zone showing the (111) lattice planes and planar defects. (b) The corresponding FFT generated from the area without the fault.

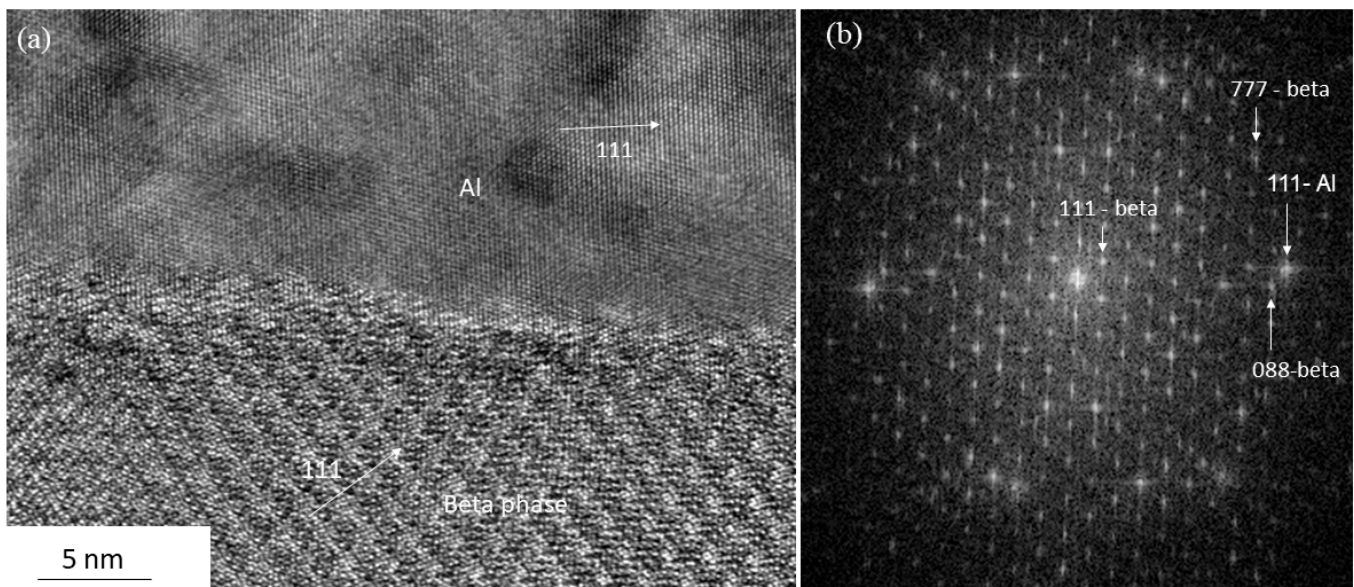


Figure 5. (a) HRTEM image showing the interface between the beta phase and matrix close to the (01-1) zone. (b) The corresponding FFT from both phases showing the (111) Al spot close to the (880) of the beta phase.

Considerable efforts have been made to understand the nucleation and growth behavior of the grain boundary beta phase. The beta phase nucleates at the grain boundary with random orientation and grows along the grain boundary in the form of a grain boundary allotriomorph via the collector plate mechanism [1]. Figure 6a shows the beta phase at the grain boundary in the early stage of growth at 100 °C. The distribution of Mg and Al and the line scan of the beta phase and the matrix is shown in Figure 6b–e. In this case, Mg atoms are mostly collected by the collector plate mechanism at the grain boundary through volume diffusion. For the beta phase to nucleate, one needs to collect a large number of Mg atoms, as a unit cell contains $0.4 \times 1168 = 467$ atoms of Mg, assuming the critical radius is close to half of the unit cell. As the volume diffusion at lower temperatures in the range of 50 to 200 °C is relatively slow, the nucleation and growth process of the beta phase also appears to be sluggish in nature. The beta phase also forms heterogeneously on top of intermetallic particles as a result of the collection of sufficient Mg atoms at the intermetallic particle/matrix interface (see Figure 7a). The high-angle annular dark field (HAADF) image shows a rod-like Al–Mn–Fe–Cr intermetallic particle with bright contrast as compared to the matrix and the beta phase with darker contrast (Figure 7b). The fine probe EDS maps showing the distribution of Mg, Al, Mn, and Cr are given in Figure 7c–f, respectively. However, the collection efficiency of Mg atoms via the dislocations or low angle boundaries is not efficient. As a result, they are unlikely to form any beta phase on dislocations or on low angle boundaries. The cell structure forms (see Figure 8) in Al5083-H131 tempered samples after extended annealing (see Figure 8) at 100 °C. The low-angle grain boundaries after sensitization at 100 °C for 14 and 45 days, respectively, are shown in Figure 8a,b. One cannot observe any beta phase at low angle grain boundaries and on dislocations.

The addition of boron changes the Al–Mg system in terms of thermodynamics and phase transformations. With boron, it solidifies via the eutectic reaction to Al (Mg, B) + Al (Mg)B₂, and becomes stable (no further decomposition) during exposure to temperatures between 50 to 200 °C. The collector plate mechanism is shown as a schematic diagram (see Figure 9), where Mg and B atoms dissolved in the matrix phase will be collected by grain boundaries. The diffusion of boron as an interstitial atom would be faster as compared to the diffusion of Mg. In addition, the collection efficiency of boron would be greater than Mg via grain boundaries at a relatively low temperature. This will most likely

result in a boride phase at grain boundaries. We, in fact, observe the boride phase (see Figure 10a,b) in Al–Mg–B samples in both as-cast as well as in annealed conditions. Note that after annealing at 150 °C for 190 h, we did not observe any significant change in the microstructure when compared to the as-cast sample.

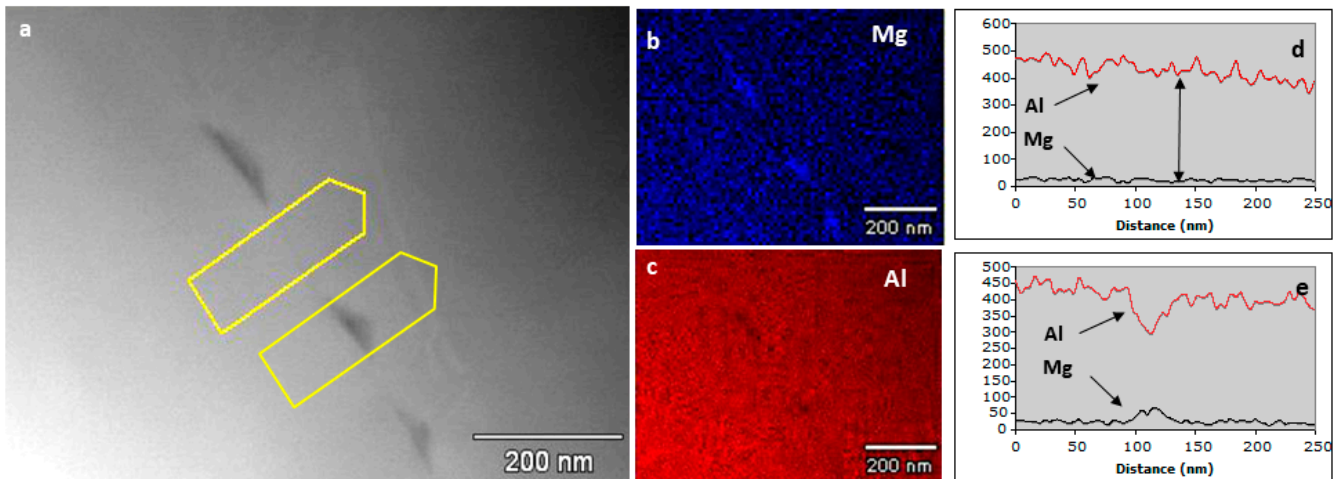


Figure 6. (a) The HAADF image showing morphology of the beta particles at grain boundary at the early stage. (b,c) The corresponding fine probe EDS maps showing the distribution of Mg and Al, respectively. (d,e) The line scans, obtained from regions indicated by yellow box arrows in Figure 6a, across the grain boundary with and without the beta phase, respectively.

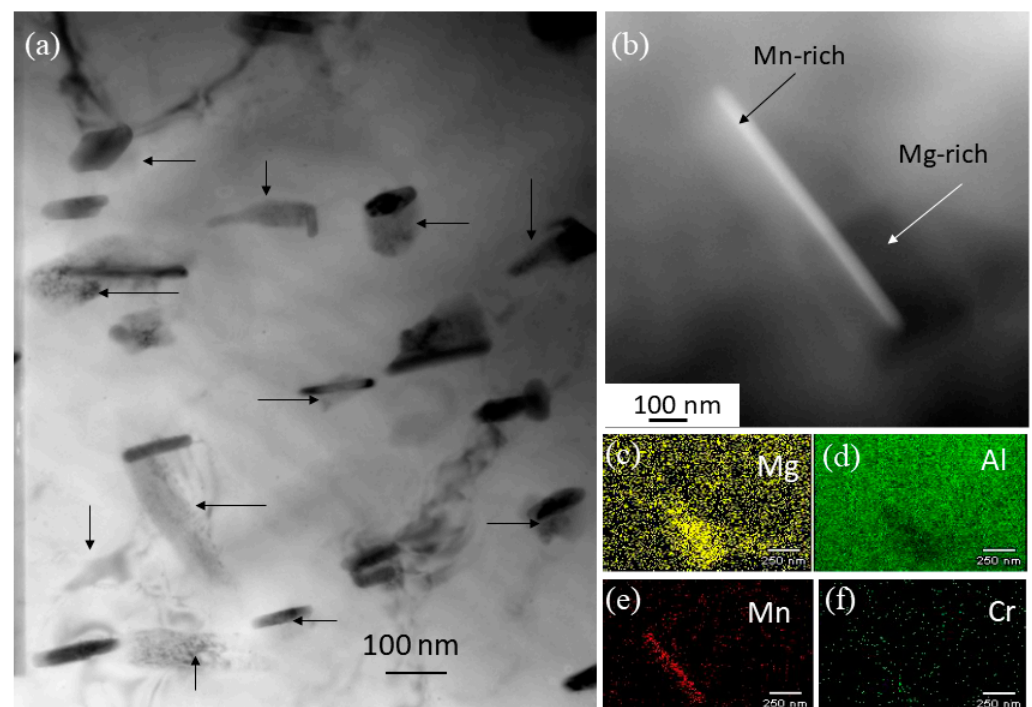


Figure 7. (a) TEM image showing the beta phase formation upon extended aging at 175 °C on top of Al–Mn–Fe–Cr type dispersoids as shown by arrows. (b) A HAADF image showing the rod-like dispersoid (bright contrast) and the beta phase (darker contrast) formed on top of the dispersoid. (c–f) The corresponding fine probe EDS maps showing the distribution of Mg, Al, Mn, and Cr, respectively, around the dispersoid particle.

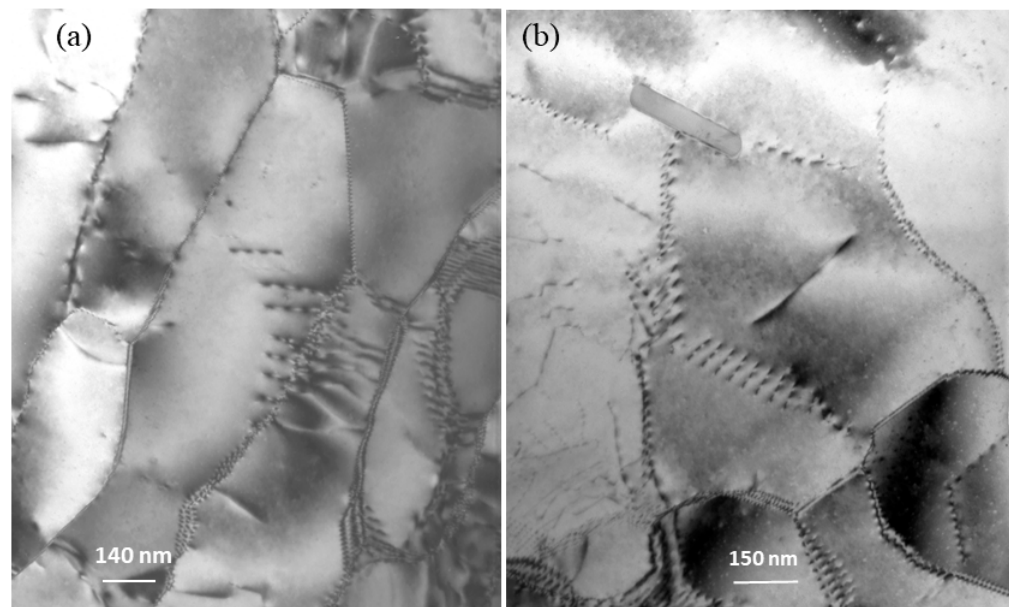


Figure 8. (a,b) The dislocation configuration at low-angle grain boundaries after sensitization at 100 °C for 14 and 45 days, respectively, showing no beta phase at low angle boundaries and on dislocations.

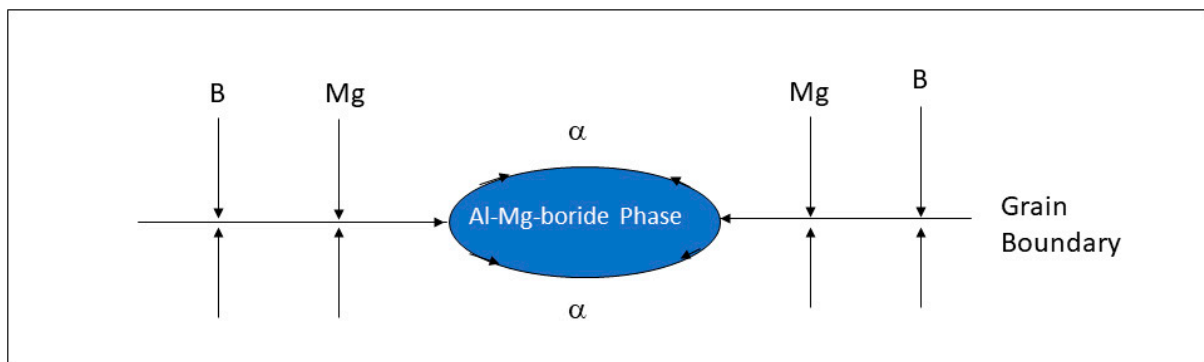


Figure 9. A schematic diagram showing the collector plate mechanism and the growth of AlMgB_2 particle.

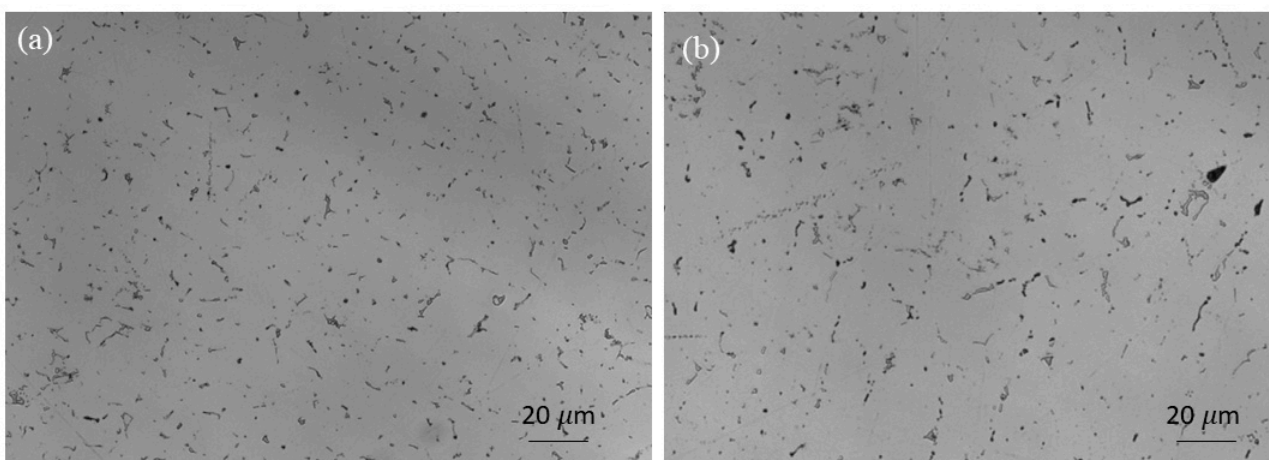


Figure 10. (a,b) Optical micrographs showing the formation of borides, which appeared dark at grain boundaries in both as-cast and as-cast + annealed conditions.

To investigate the nature of the di-boride phase, we performed HAADF imaging, fine probe EDS mapping, and XRD and HRTEM imaging. Figure 11a is a HAADF image of a rod-like boride particle in an Al matrix. The fine probe EDS maps from this particle shows the distribution of Al, B, and Mg (Figure 11b–d), respectively. Note that MgB_2 is isostructural with AlB_2 and some solubility of magnesium in AlB_2 lattice would be expected. The Mg will substitute the Al atoms in the AlB_2 lattice. From XRD scans (see Figure 12), one could observe the fcc-Al (Mg) and an AlMgB_2 phase. In Figure 12, we illustrate XRD from sample containing 3 wt.% B in the annealed condition showing Al reflections. A small peak at $2\theta = 44.25^\circ$ indexed as (10-11) from the AlMgB_2 phase close to the (200) of Al has been observed. Figure 13a shows a low magnification TEM image of a rod-like boride particle. The HRTEM of the portion of the rod particle is shown in Figure 13b close to the (11-20) zone showing the (0001) and (10-10) lattice planes of the di-boride phase. The corresponding FFT is shown by Figure 13c.

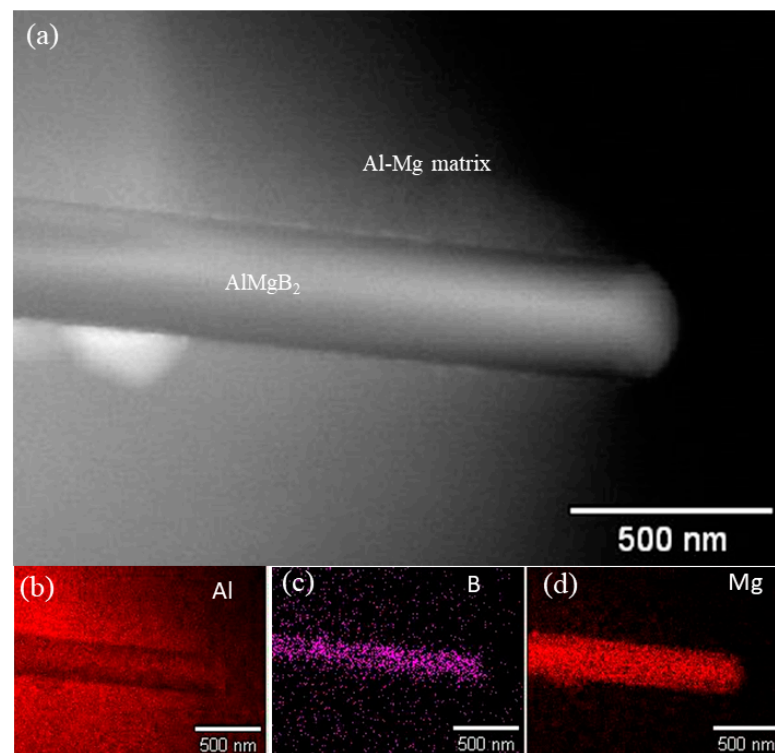


Figure 11. (a) HAADF image showing a rod-like boride particle. (b–d) The corresponding fine probe EDS maps showing the distributions of Al, B, and Mg, respectively.

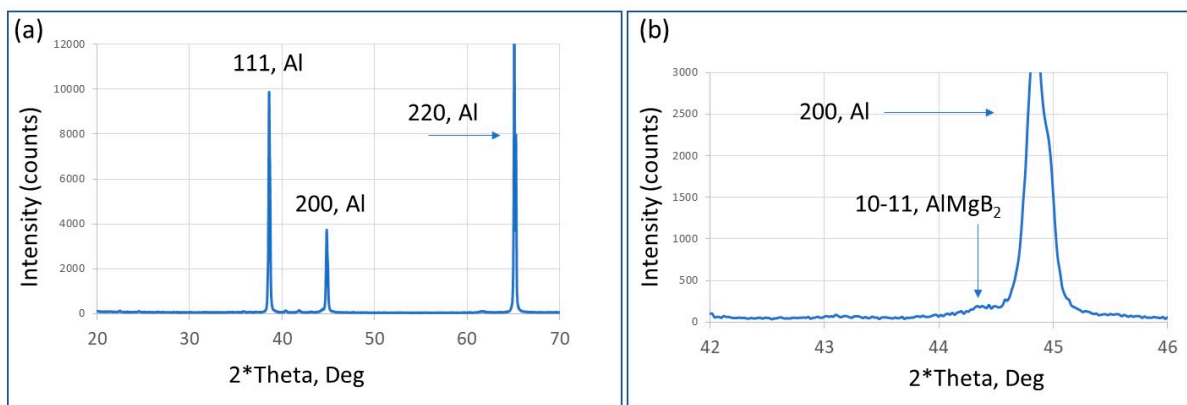


Figure 12. (a) XRD from sample containing 3 wt.% B in the annealed condition showing the Al reflections. (b) A tiny peak from the AlMgB_2 phase close to the (200) of Al can be observed.

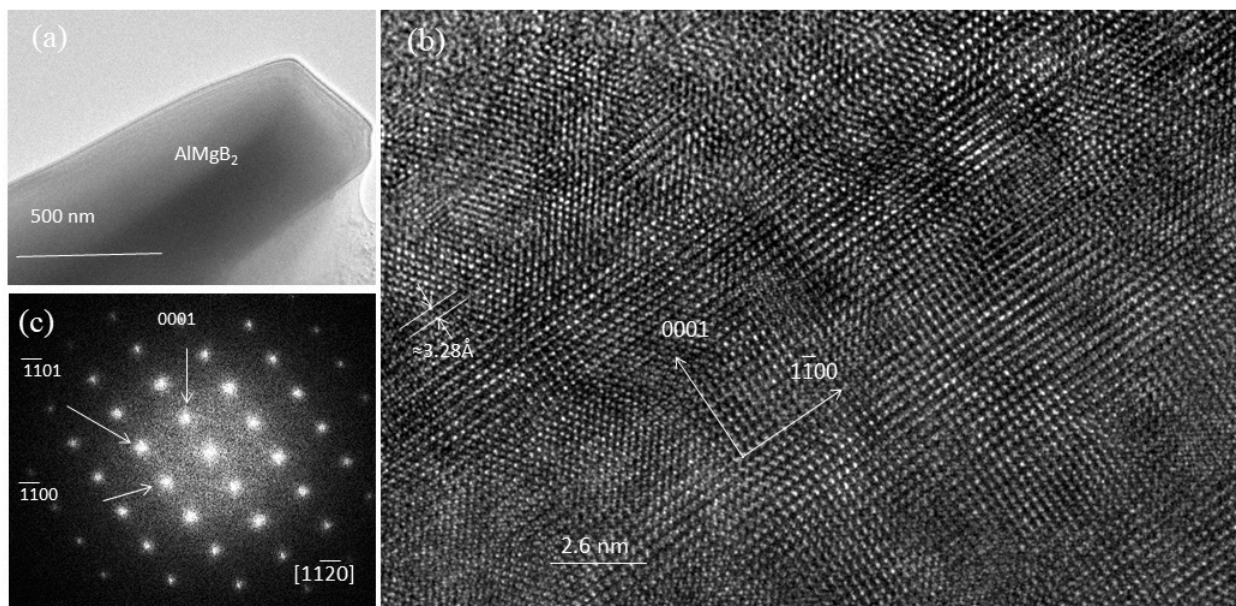


Figure 13. (a) TEM image of a rod-like boride. (b) The corresponding HRTEM image close to the (11–20) zone. (c) The FFT from the HRTEM image.

We studied the hardness of the Al 5083-B with 1, 2, and 3 wt.% boron and compared it with the hardness of Al 5083 in as-received and annealed conditions. In the as-received condition, the average Vickers (HV) hardness of Al 5083 was 97. Upon annealing at 175 °C for around 100 h, the hardness decreased to 90 (see Figure 14a). Our previous studies [2,3] show that, upon annealing, magnesium exits the solid solution and precipitates out as a beta phase at grain boundaries. For Al 5083 with 1 wt.% boron in the as-cast condition, the average Vickers hardness was 87. With the increase in boron content to 3 wt.%, the average hardness decreases to 82 (see Figure 14b). This suggests that the matrix has been depleted with magnesium as a result of the formation of di-boride phase in the matrix.

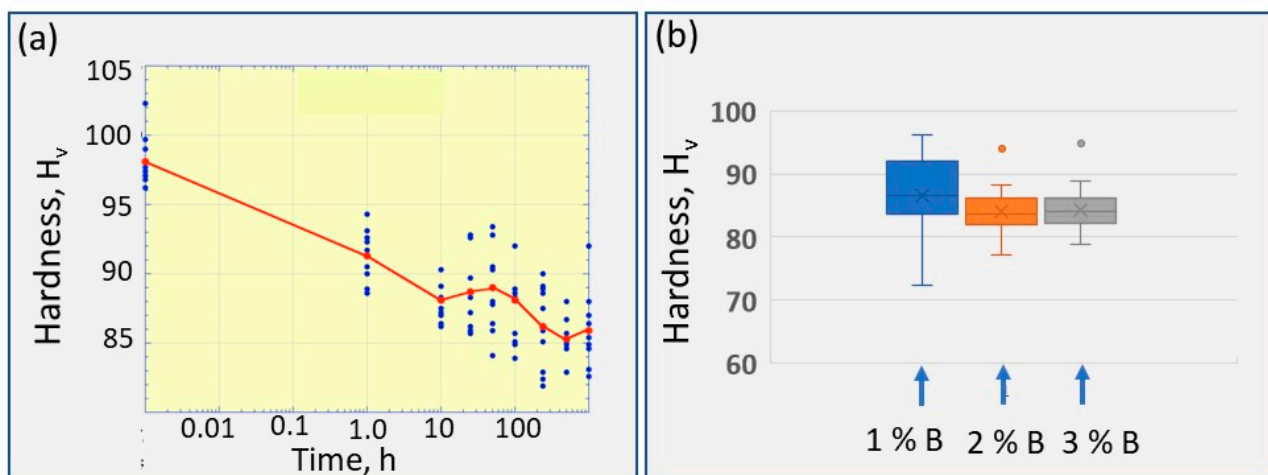


Figure 14. (a) Vickers hardness of Al 5083 as a function of aging at 100 °C, showing the decrease in hardness. (b) Vickers hardness with boron additions. Different color dots in Figure 14b represent different boron levels.

To study the intergranular corrosion behavior of the boride phase, samples with 3 wt.% boron containing the boride phase were immersed in saltwater (3 wt.% NaCl) for a week at room temperature. Figure 15a,b shows the microstructure after the salt exposure in the as-cast and annealed conditions, respectively. We did not observe any dissolution

of the boride phase after saltwater exposure. This can be contrasted with the saltwater immersion treatment of the sensitized Al 5083 sample without any boron content, and one can observe the significant dissolution of the beta phase after the saltwater exposure at room temperature for a week (see Figure 3b). This suggests that the AlMgB_2 phase is not anodic with respect to the Al matrix and is resistant to intergranular corrosion. To quantify and compare the dissolution characteristics, we carried out a nitric acid mass loss test for samples with 3 wt.% boron and samples without boron. We estimate the mass loss to be 4 mg/cm^2 in Al5083 with boron while the mass loss of a fully sensitized sample without boron is 45 mg/cm^2 .

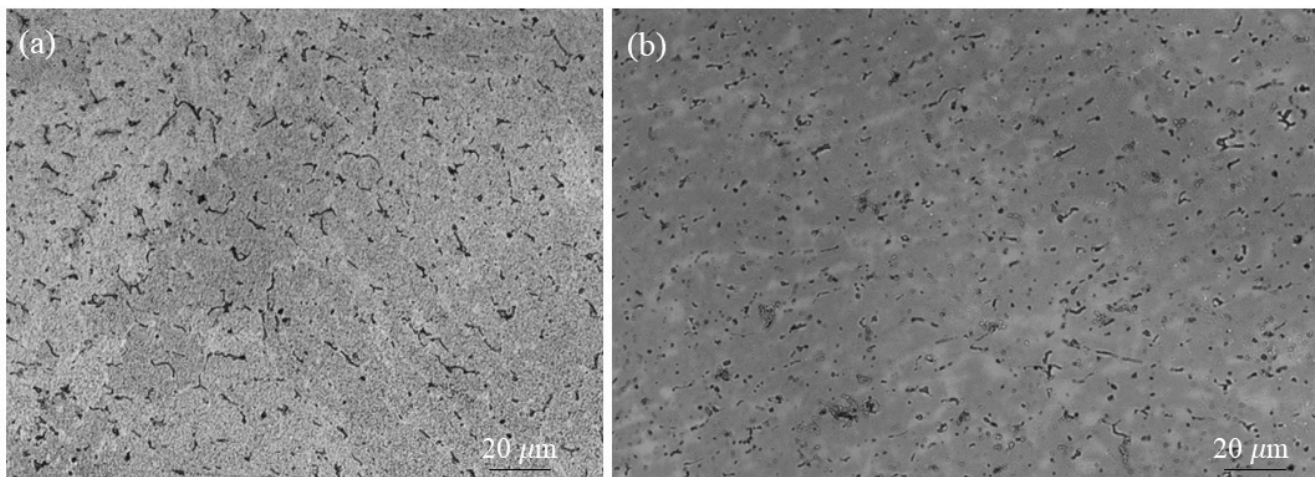


Figure 15. (a,b) Optical micrographs after saltwater immersion for a week showing no dissolution of borides at grain boundaries in as-cast and as-cast + annealed conditions, respectively. The di-boride appears as dark particles.

In this work, we manufactured Al5083-B alloys with boron ranging from 0.5 to 3 wt.%. It was observed that the hardness (see Figure 14b) of Al5083-B alloys decreases with the increase in boron content. Future work is in progress to optimize the boron content, although a small amount of boron would be adequate for desensitization. It would be reasonable to keep the boron level within 0.5 to 1 wt.% or below.

4. Summary and Conclusions

We demonstrated that the beta phase formation in aluminum–magnesium alloys has been suppressed via alloying with small amounts of boron. This is a significant finding as it provides a new insight into how to minimize the longstanding problem of sensitization in aluminum–magnesium alloys. The following conclusions can be made.

1. TEM and XRD revealed that a boride compound, AlMgB_2 , forms within the aluminum matrix, which reduces the supersaturation of magnesium in the aluminum matrix. The beta phase, Al_3Mg_2 , does not nucleate and grow at grain boundaries upon extended annealing at 150°C .
2. The AlMgB_2 compound formed at grain boundaries does not dissolve in saltwater, suggesting that it is less anodic relative to the Al matrix and resistant to intergranular corrosion.
3. The estimated mass loss obtained using the nitric acid mass loss testing is 4 mg/cm^2 for boron containing Al5083 aged at 150°C for 190 h as compared to the mass loss of 45 mg/cm^2 for a fully sensitized Al5083 without boron, suggesting that the addition of boron is highly effective in suppressing the susceptibility to intergranular corrosion in Al5000 series alloys.

Author Contributions: Conceptualization, R.G.; methodology, R.G., S.B.Q. and R.L.H.; formal analysis, R.G., S.B.Q. and R.L.H.; investigation, R.G.; resources, A.G. and A.M.; writing—original draft preparation, R.G.; writing—review and editing, A.M. and R.G.; visualization, R.G.; supervision, R.L.H. and A.G.; project administration, R.G. and R.L.H.; funding acquisition, R.G., R.L.H. and A.G. All authors have read and agreed to the published version of the manuscript.

Funding: Funding for this project was provided by the Office of Naval Research (ONR) through the Naval Research Laboratory's 6.1 Research Program.

Data Availability Statement: The data presented in this study are available in article.

Conflicts of Interest: The authors declare no conflict of interest.

Distribution Statement A: Approved for public release, distribution is unlimited.

References

1. Goswami, R.; Spanos, G.; Pao, P.S.; Holtz, R.L. Precipitation Behavior of the Beta Phase in Al 5083. *Mater. Sci. Eng. A* **2010**, *527*, 1089–1095. [[CrossRef](#)]
2. Goswami, R.; Pao, P.S.; Spanos, G.; Holtz, R.L. Microstructural Evolution and Stress Corrosion Cracking Behavior of Al-5083. *Metall. Trans. A* **2011**, *42*, 348–355.
3. Goswami, R.; Holtz, R.L. Transmission Electron Microscopic Investigations of Grain Boundary Beta Phase Precipitation Behavior in Al 5083 Aged at 373K (100 C). *Metall. Trans. A* **2013**, *44*, 1279–1289. [[CrossRef](#)]
4. Zhang, R.; Knight, S.P.; Holtz, R.L.; Goswami, R.; Davies, C.H.; Birbilis, N. A Survey of Sensitization in 5xxx Series Aluminum Alloys. *Corros. Sci.* **2016**, *72*, 144–159. [[CrossRef](#)] [[PubMed](#)]
5. Goswami, R.; Pao, P.S.; Qadri, S.B.; Holtz, R.L. Severe plastic deformation induced sensitization of cryo-milled nanocrystalline Al-7.5 Mg. *Metall. Mater. Trans. A* **2014**, *45*, 2894–2898. [[CrossRef](#)]
6. Bernstein, N.; Goswami, R.; Holtz, R.L. Surface and interface energies of complex crystal structure aluminum magnesium alloys. *Metall. Mater. Trans. A* **2015**, *43*, 2166–2176. [[CrossRef](#)]
7. Holtz, R.L.; Pao, P.S.; Bayles, R.A.; Longazel, T.M.; Goswami, R. Corrosion fatigue of Al 5083-H131 sensitized at 70, 100, and 175 °C relation to microstructure and degree of sensitization. In Proceedings of the DoD Corrosion Conference, Houston, TX, USA, 13–17 March 2011; NACE/DoD.
8. Sethian, J.D.; Myers, M.C.; Wolford, M.; Hegeler, F.; Holtz, R.L.; Horton, D.; Lewis, A.C.; Wahl, K.J. Desensitization of Aluminum Alloys Using Pulsed Electron Beams. U.S. Patent US9315886B1, 19 April 2016.
9. Holtz, R.L.; Horton, D. Surface Metallographic Method for Characterizing the Degree of Sensitization of Aluminum-Magnesium Alloys. U.S. Patent US9898832B1, 20 February 2018.
10. Juneidi, N.; Asha, R.; Jarrar, F.; Ozturk, F. Design for Manufacturing of an Aluminum Superplastic AA5083 Alloy Plate-Fin Heat Exchanger. *J. Mater. Sci. Res.* **2016**, *5*, 122–127.
11. Kramar, L.; Phillippi, M.; Tack, W.T.; Wong, C. Locally Reversing Sensitization in 5xxx Aluminum Plate. *J. Mater. Eng. Perform.* **2012**, *21*, 1025–1029. [[CrossRef](#)]
12. Taheri, M.L.; D'Antuono, D.S. Annealing Process. U.S. Patent US20160186301A1, 30 June 2016.
13. Halap, A.; Radetic, T.; Popovic, M.; Romhanji, E. Intergranular Corrosion Susceptibility of an AA5083 Al-Mg Alloy Processed by Accumulative Roll Bonding (ARB). *Metall. Mater. Trans. A* **2014**, *45*, 4572–4579. [[CrossRef](#)]
14. Argade, G.R.; Kumar, N.; Mishra, R.S. Stress Corrosion Cracking Susceptibility of Ultrafine Grained Al-Mg-Sc Alloy. *Mat. Sci. Eng. A* **2013**, *565*, 80–89. [[CrossRef](#)]
15. Sharma, M.M.; Ziemian, C.W. Pitting and Stress Corrosion Cracking Susceptibility of Nanostructured Al-Mg Alloys in Natural and Artificial Environments. *J. Mater. Eng. Perform.* **2008**, *17*, 870–878. [[CrossRef](#)]
16. Sikora, E.; Wei, X.J.; Shaw, B.A. Corrosion Behavior on Nanocrystalline Bulk Al-Mg-Based Alloys. *Corrosion* **2004**, *60*, 387–398. [[CrossRef](#)]
17. Gupta, R.K.; Zhang, R.; Davies, C.H.J.; Birbilis, N. Theoretical Study of the Influence of Microalloying on Sensitization of AA5083 and Moderation of Sensitization of a Model Al-Mg-Mn Alloy via Sr Additions. *Corrosion* **2014**, *70*, 402–413. [[CrossRef](#)] [[PubMed](#)]
18. Wang, Y.; Gupta, R.K.; Sukiman, N.L.; Zhang, R.; Davies, C.H.; Birbilis, N. Influence of alloyed Nd content on the corrosion of an Al-5Mg alloy. *Corros. Sci.* **2013**, *73*, 181–187. [[CrossRef](#)]
19. Goswami, R.; Lynch, S.; Holroyd, N.J.; Knight, S.P.; Holtz, R.L. Evolution of grain boundary precipitates in Al 7075 upon aging and correlation with stress corrosion cracking behavior. *Metall. Mater. Trans. A* **2013**, *44*, 1268–1278. [[CrossRef](#)]
20. McMahan, M.E.; Burns, J.T.; Scully, J.R. Development of new criteria for evaluating the effectiveness of Zn-rich primers in protecting Al-Mg alloys. *Prog. Org. Coat.* **2019**, *135*, 392–409. [[CrossRef](#)]
21. Goswami, R.; Qadri, S.B. Suppression of Samson Phase Formation in Al-Mg Alloys by Boron Addition. *Mater. Lett.* **2017**, *200*, 21–23. [[CrossRef](#)]
22. Goswami, R.; Qadri, S.B. Suppression of Samson Phase Formation in Al-Mg Alloys by Boron Addition. U.S. Patent US11028462, 8 June 2021.

23. Goswami, R.; Qadri, S.B. Investigation of Fine-Scale Microstructure and Mechanical Behavior of Al-Mg-B and Al-Mg-Cd Composites for Intergranular Corrosion Protection Applications. In *Metal-Matrix Composites: Advances in Processing, Characterization, Performance and Analysis*; Springer International Publishing: Cham, Switzerland, 2022; pp. 145–153.
24. Samson, S. The Crystal Structure of the Phase β Mg₂Al₃. *Acta Crystallogr.* **1965**, *19*, 401–413. [[CrossRef](#)]
25. Feuerbacher, M.; Thomas, C.; Makongo, J.P.A.; Carrillo-Cabrera, W.; Cardoso, R.; Grin, Y.; Kreiner, G.; Joubert, J.-M.; Schenk, T.; Gastaldi, J.; et al. The Samson phase, β -Mg₂Al₃, revisited. *Z. Kristallogr.* **2007**, *222*, 259–288.

Disclaimer/Publisher's Note: The statements, opinions and data contained in all publications are solely those of the individual author(s) and contributor(s) and not of MDPI and/or the editor(s). MDPI and/or the editor(s) disclaim responsibility for any injury to people or property resulting from any ideas, methods, instructions or products referred to in the content.